Published in final edited form as:
J Phys Chem A. 2009 May 14; 113(19): 5710–5717. doi:10.1021/jp900402y.

Cleavage of [4Fe-4S]-Type Clusters: Breaking the Symmetry

Shuqiang Niu and **Toshiko Ichiye***
Department of Chemistry, Georgetown University, Washington, DC 20057-1227

Abstract

The cleavage of [4Fe-4S]-type clusters is thought to be important in proteins such as Fe-S scaffold proteins and nitrogenase. However, most $[4Fe\text{-}4S]^{2+}$ clusters in proteins have two antiferromagnetically coupled high-spin layers in which a minority spin is delocalized in each layer, thus forming a symmetric $Fe^{2.5+}$-$Fe^{2.5+}$ pair, and how cleavage occurs between the irons is puzzling because of the shared electron. Previously we proposed a novel mechanism for the fission of a [4Fe-4S] core into two [2Fe-2S] cores in which the minority spin localizes on one iron, thus breaking the symmetry and creating a transition state with two Fe^{3+}-Fe^{2+} pairs. Cleavage first through the weak Fe^{2+}—S bonds lowers the activation energy. Here, we propose a test of this mechanism: break the symmetry of the cluster by changing the ligands to promote spin localization, which should enhance reactivity. The cleavage reactions for the homo-ligand $[Fe_4S_4L_4]^{2-}$ (L = SCH_3, Cl, H) and hetero-ligand $[Fe_4S_4(SCH_3)_2L_2]^{2-}$ (L = Cl, H) clusters in the gas phase were examined via broken-symmetry density functional theory calculations. In the hetero-ligand clusters, the minority spin localized on the iron coordinated by the weaker electron donor ligand and the reaction energy and activation barrier of the cleavage were lowered, which is in accord with our proposed mechanism and consistent with photoelectron spectroscopy and collision-induced dissociation experiments. These studies suggest that proteins requiring facile fission of their [4Fe-4S] cluster in their biological function might have spin-localized [4Fe-4S] clusters.

Introduction

The cuboidal [4Fe-4S] cluster found in metalloproteins are ubiquitous and multipurpose in biological systems.[1–3] The most widely recognized function of iron-sulfur clusters is as electron carriers in numerous electron transfer proteins found in bioenergetic pathways such as photosynthesis and respiration. The wide range of reduction potentials for a given cluster type appears to be mainly a function of the protein environment.[4–12] More recently, the [4Fe-4S] core has been found to play important roles in regulation, sulfur and iron transport, and sensing.[3,13–15] The ability of these clusters to play so many roles comes in part from variations in their unusual electronic and bonding structure. One unique feature is that the [4Fe-4S] core can be cleaved to either a [3Fe-4S] or two [2Fe-2S] cores. For instance, in the proposed mechanism for the assembly of [4Fe-4S] clusters in some proteins, a transient [4Fe-4S] cluster is assembled on cysteine residues of a scaffold protein and then one [2Fe-2S] layer at a time is transferred to a target protein.[16–23] Also, the [4Fe-4S] cluster in a nitrogenase Fe-protein can convert to two [2Fe-2S] clusters.[24] Exploring the mechanism of the cleavage is essential in understanding the function of these proteins. Moreover, since clusters that act as redox sites are relatively stable while others require facile fission for their function,

*To whom correspondence may be addressed. E-mail: ti9@georgetown.edu.

Supporting Information Available: The optimized geometry (Table S1) and Mülliken charges and spin density (in e^-) (Table S2) of the clusters, the Mülliken spin density of the transition states and half-cleaved intermediates (Table S3 and Table S4) and the relative isomerization energies of the hetero-ligand clusters (Table S5). This material is available free of charge via the Internet at http://pubs.acs.org.

determining the factors that control cluster fission are crucial for understanding their structure-function relationships.

The symmetric fission of the $[4Fe\text{-}4S]^{2+}$ core into two [2Fe-2S] cores presents an interesting conundrum because of the distinctive spin structure exhibited by the standard $[Fe_4S_4(Cys)_4]^{2-}$ cluster found in Fe-S proteins. Mössbauer and EPR spectroscopy[1] and electronic structure calculations[25] support that the $[4Fe\text{-}4S]^{2+}$ core consists of two high-spin (S_i = 9/2) ferromagnetic $[2Fe\text{-}2S]^{+}$ layers, which are coupled antiferromagnetically to form a low-spin (S = 0) cubic structure (Scheme 1a). In each layer, the minority spin (s = 1/2) is the highest occupied molecular orbital (HOMO) electron and is delocalized between two iron sites, which generates additional stabilizing energy and creates a symmetric $Fe^{2.5+}$-$Fe^{2.5+}$ pair.[26] Since the antiferromagetic coupling holding the two layers together is stronger than the spin double exchange interactions holding a given layer together, fission by cleaving both layers in half perpendicular to the planes (Scheme 1b) should be lower in energy than fission between the layers (Scheme 1c). Moreover, cleavage between the layers would result in high-spin [2Fe-2S] cores, contrary to experiment. However, the delocalization of the minority spin between the two irons in a layer would seem to preclude cleaving perpendicular to the layers since the spin cannot be divided evenly between the two irons, thus leading to the question of the mechanism for this cleavage reaction.

Because of the complexity of this problem, valuable insights can be provided by our broken-symmetry (BS) density functional theory (DFT) studies[26–29] in conjunction with photoelectron spectroscopy (PES) and other experiments by Wang and coworkers on $[4Fe\text{-}4S]$[30–34] and other clusters,[34–38] which are providing a fundamental understanding of these clusters and the effects of the protein environment on them. Since both theory and experiment are of cluster analogs in the gas phase, the DFT calculations do not require approximations for the environment such as solvent corrections or a protein matrix. In our studies of the fission of the $[Fe_4S_4Cl_4]^{2-}$ cluster into two $[Fe_2S_2Cl_2]^{-}$clusters,[27,28] we proposed a novel mechanism involving spin localization. In the first step, the minority spin of a layer localizes on one of the irons to create a spin-localized transition structure with Fe^{3+}-Fe^{2+} pairs. Next the two sets of weaker Fe^{2+}—S bonds cleave perpendicularly to the layers to generate a half-cleaved cluster, and finally the second set of bonds cleave to form the $[2Fe\text{-}2S]^{+}$ products.[28] Thus, this mechanism implies that clusters with a lower spin double exchange interaction; i.e., greater spin-localization, should cleave more readily.

A test of this mechanism is to enhance magnitude of the minority spin-localization, which should increase the reactivity to cleavage. Since a useful strategy for studying the physical origins of the effects of the protein on the properties of the clusters has been to design cluster ligands that either mimic[39,40] or exaggerate[24] different types of physical interactions, ligands that break the symmetry of the layers may promote localization of the minority spin. Furthermore, [4Fe-4S] clusters in proteins that undergo facile conversion to [3Fe-4S] clusters are often coordinated by one noncysteinyl ligand such as an aspartate in some ferredoxins[41–46] and water in aconitase[3,14] , pyruvate formate-lyase.[47] Interesting, the [4Fe-4S] cluster coordinated by an *S*-adenosylmethionine (SAM)[48–51] in the radical-SAM enzymes converts to a [3Fe-4S] cluster in pyruvate formate-lyase[47] but to one [2Fe-2S] core in biotin synthase.[52] Moreover, a cysteine to serine mutant (C77S) of the *Chromatium vinosum* high potential iron-sulfur protein leads to shift in the electron cloud of the cluster toward the serine[53–56], indicating that ligand substitution alters the electron distribution. Thus, defining the role of ligand hetereogeneity in fission not only provides a test of the mechanism, but also is essential in understanding the structure-function relationships of Fe-S proteins.

Here, the mechanism was tested by breaking the symmetry of the ligation of the [4Fe-4S] cluster to promote spin localization, utilizing BS-DFT calculations in conjunction with findings

of PES and collision-induced dissociation (CID) experiments[31]. Previous PES and DFT studies indicate that $[Fe4S4L4]^{2-}$ (L = SC_2H_5, SH, Cl, Br, I) clusters have similar electronic structure and other properties to the $[Fe_4S_4(Cys)_4]^{2-}$cluster found in proteins,[26] with variations due to the electron donating ability of the terminal ligands since the minority spin is delocalized in the $\sigma_{Fe—Fe}$ orbitals, which also have $\sigma^*_{Fe—S}$ and $\sigma^*_{Fe—L}$ antibonding character.[26] Assuming coordination by identical ligands on a layer promotes the delocalization of the minority spin between the irons are equivalent, coordination by different ligands with different electron donor properties may increase the localization of the minority spin on one iron by breaking the symmetry. Comparison of $[Fe_4S_4(SCH_3)_2L_2]^{2-}$ (L = Cl, H) with $[Fe_4S_4L_4]^{2-}$ (L = SCH_3, Cl, H) in the reactant and a half-cleaved intermediate state indicates that hetero-ligand coordination promotes minority spin-localization and further that spin-localization lowers the barrier to fission.

Methods

Since the systems here involve antiferromagnetically spin-coupled interactions, the BS approach[57,58] for the DFT calculations[59] was employed to take these interactions into account in the exchange-correlation energy functionals. Becke's three-parameter hybrid exchange[60] and Lee−Yang−Parr correlation functional (B3LYP)[61] using the 6–31G** basis sets[62–64] was utilized for the geometry optimizations and electronic structure calculations of the [4Fe-4S] clusters. The calculated oxidation energies were refined at the B3LYP/6–31(++)$_S$G**// B3LYP/6–31G** level, where (++)$_S$ indicates that *sp*-type diffuse functions were added to the basis set for the sulfur atoms.[62–64] Previous studies indicate that this approach significantly improved the accuracy of the calculated redox energies.[26,28,37] In addition, zero point energy and entropic terms at 298 K were calculated at the B3LYP/6–31G** level. The σ electron donating ability of the ligands was assessed by the calculated proton affinity (PA) of the ligand alone at the B3LYP/6–31G** level; i.e., ligands with greater proton affinity should donate more σ electron density.

Transition states (TS) were optimized by an eigenvalue-following optimization method,[65] in which the final updated Hessian[66] has only one negative eigenvalue with eigenvectors representing the Fe—S bond formation and cleavage. Further optimizations along an intrinsic reaction coordinate based on the Hessian calculated above and frequency calculations were used to confirm the reaction pathways. No symmetry restraints were imposed during geometry optimizations. Although the energy of a BS state for a spin polarized low-spin state is not the energy of a pure spin state because a single determinant is used, it can be corrected by an approximate spin projection procedure.[25,67] On the other hand, since a BS state is a weighted average of pure-spin states, the potential energy surface of a ground state with large spin numbers is close to that of the true ground state. Previous BS-DFT calculations of $[Fe_2S_2(SCH_3)_4]^{2-}$ indicate that the projection corrected values of 2.68 Å for the Fe—Fe distance are excellent agreement with experimental value of 2.69 Å; however, there is no automated method for adding the projection correction to the geometry optimization and the uncorrected value leads to a systematic increase in the Fe—Fe distance of only ~ 0.1 Å.[68] Moreover, the spin projection corrections tend to cancel for oxidation or reaction energies. For instance, the projection corrections on $[Fe4S4Cl4]^{2-}$ at the B3LYP/6–31(++)$_S$G**//B3LYP/ 6–31G** level lead to a decrease of 0.01 and 0.04 eV in the vertical (VDE) and adiabatic (ADE) detachment energies, respectively, which actually increase the deviation from experiment, and a decrease of 0.34 kcal/mol in the half-cleavage reaction energy. Thus, the spin projection procedures were neglected in this work.

All calculations were performed using the NWChem program package.[69] The molecular orbital visualizations were performed using the extensible computational chemistry environment (Ecce) application software.[70]

Results and Discussion

The electronic structure of the $[4Fe\text{-}4S]^{2+}$ core is expected to depend on the electron donating ability of the terminal ligands since the minority spin is delocalized in the $\sigma_{Fe—Fe}$ orbitals, which also has metal-ligand character,[26] and the electron donating ability should increase with decreasing proton affinity (PA). The calculated oxidation energies of the [4Fe-4S] clusters are in good agreement with experiment and also correlate well with the proton affinities of the ligands of $[Fe_4S_4L_4]^{2-}$ (L = $SC_2H_5^-$, SH^-, Cl^-, Br^-, I^-) (Figure 1). Furthermore, in a layer bonded by ligands with different PA, the Fe ligated by the poorer **a** electron donor should have less electron density and more Fe^{3+} character than the other Fe, thus breaking the symmetry of the system. Consequently, the hetero-ligand clusters may exhibit less delocalization of the minority spin and thus greater reactivity than the homo-ligand clusters. A comparison is made here between the homo-ligand clusters $[Fe_4S_4L_4]^{2-}$ (L = SCH3, Cl, H) and the hetero-ligand clusters $[Fe_4S_4(SCH_3)_2L_2]^{2-}$ (L = Cl, H) (Scheme 2). Two isomers are possible for the hetero-ligand clusters depending on which irons the minority spins are located on, resulting in homo-ligand layers, denoted as $[Fe_4S_4(SMe)_2L_2]^{2-}$ (Scheme 2b) or hetero-ligand layers, denoted as $[Fe_4S_4(SMe,L)_2]^{2-}$ (Scheme 2c), where SMe refers to SCH_3. The notation $[Fe_4S_4(SCH_3)_2L_2]^{2-}$ will refer to either isomer.

Electron Detachment Energy of Cubic [4Fe-4S]

The calculated ADE and VDE of the hetero- and homo-ligand clusters were in good agreement with available experimental PES results (Table 1).[34] For $[Fe_4S_4Cl_4]^{2-}$, the weaker electron donor chloride ligand lowered the energy of the minority spin orbitals, consequently increasing the electron detachment energy by ~ 0.5 eV with respect to $[Fe_4S_4(SCH_3)_4]^{2-}$. Conversely, for $[Fe_4S_4H_4]^{2-}$, the much better electron donor hydride ligand decreased the detachment energy by ~ 0.6 eV with respect to $[Fe_4S_4(SCH_3)_4]^{2-}$. The calculated oxidation energies of either of the two possible isomers of the $[Fe_4S_4(SCH_3)_2Cl_2]^{2-}$ were similar to and in good agreement with experiment; however, the calculations indicate that $[Fe_4S_4(SMe,L)_2]^{2-}$was slightly more stable for L = H and Cl by 0.87 and 0.81 kcal/mol, respectively, than $[Fe_4S_4(SMe)_2L_2]^{2-}$ (*see infra*). Overall, the detachment energy of the [4Fe-4S] cores correlated with electron donor properties of the terminal ligands on the layer, increasing in the order HH < SMeH < SMeSMe < SMeCl < ClCl.

$Fe^{2.5+}$-$Fe^{2.5+}$ versus Fe^{3+}-Fe^{2+} Character

The $Fe^{2.5+}$-$Fe^{2.5+}$ versus Fe^{3+}-Fe^{2+} character of the layers as a function of ligand type was examined by the length of the Fe—S bonds within a layer (Figure 2 and Table S1 and Table S2). Previous results have shown that the BS-DFT calculations in the gas phase predict Fe—S bonds that are too long by ~0.05 Å, which is a systematic error using the B3LYP functional, but show the correct trends of lengthening upon reduction from Fe^{3+}—S to Fe^{2+}—S in comparison to X-ray structures;[26,28,37] i.e., the calculated Fe^{3+}—S bond length of 2.23—2.37 Å, the $Fe^{2.5+}$—S bond length of 2.36—2.37 Å, and the Fe^{2+}—S bond length of 2.40—2.47 Å, are comparable with the experimental values of 2.20—2.27 Å,[71,72] 2.28—2.32 Å,[72–74] and 2.32—2.36 Å,[71,73,75] respectively. The $Fe^{2.5+}$-$Fe^{2.5+}$ versus Fe^{3+}-Fe^{2+} character of the layers as a function of ligand character was also examined by the Mülliken charge (Figure 3a and Table S2) and the spin densities (Figure 3b and Table S2) of the irons.

The clusters with a symmetric ligation pattern for each layer, i.e., $[Fe_4S_4L_4]^{2-}$ and the $[Fe_4S_4(SMe)_2L_2]^{2-}$ isomers, were examined first. The calculated intralayer Fe—S bonds were ~2.36 Å, consistent with $Fe^{2.5+}$—S bonds. In addition, the bond lengths increased slightly with increasing electron donating ability of the terminal ligands in the order $Cl^- < SCH_3^- < H^-$, which indicated electron density shifting from the ligand to the iron, leading to increasing Fe^{2+} character of the Fe—S bonds (Figure 2a), in very good agreement with the experimental

results (Figure 2b).[71,73,75] Moreover, for a given Fe, the Mülliken charge decreased (Figure 3a) and the magnitude of the spin density increased (Figure 3b) with increasing Mülliken charge on its terminal ligand, indicating that electron density shifted from the ligand to the iron to increase its Fe^{2+} character. Thus, the results all indicated that the irons with terminal ligands with greater electron donating ability had greater Fe^{2+} character, although of course the trends may be altered in a solvent environment.

The clusters with different ligands on each layer, i.e., the $[Fe_4S_4(SMe,L)_2]^{2-}$isomers, showed significant differences from clusters with the symmetric ligation layers. For the calculated intralayer Fe—S bonds of $[Fe_4S_4(SMe,Cl)_2]^{2-}$, the irons ligated by Cl^- appeared to form Fe^{2+}—S bonds while the irons ligated by SCH_3^- appeared to form Fe^{3+}—S bonds and for $[Fe_4S_4(SMe,H)_2]^{2-}$, the irons ligated by H^- appeared to form Fe^{3+}— S bonds while the irons ligated by SCH_3^- appeared to form Fe^{2+}—S bonds (Figure 2a). This tendency is also seen X-ray structures (Figure 2b) of other mixed ligand clusters;[71,73,75] however, the differences in Fe—S bond length are smaller apparently due to smaller differences in electron donating ability of the ligands in these compounds or other factors such as the aromatic phenyl group of SPh^-. Thus, hetero-ligand coordination on a layer apparently resulted in a set of Fe^{3+}—S and Fe^{2+}—S bonds in that layer but unlike the homo-ligand case, the Fe—S bond length decreased with increasing electron donating ability of the ligand so that the iron coordinated with the better electron donor ligand had greater Fe^{3+} character of its Fe—S bond than the iron coordinated with the poorer electron donor ligand. The correlation the Mülliken charge and the magnitude of the spin density with the Fe^{2+}/Fe^{3+} character of the irons is more difficult to understand, in part because the minority spin is of opposite sign to the majority spins so that greater spin density can mean either more electron donation from the ligand or less contribution of the minor spin electron. However, the relative Mülliken charges and the magnitudes of the spin density of the two irons on a layer were generally consistent with the iron coordinated with the better electron donor ligand having greater Fe^{3+} character, just as in the bond lengths. Moreover, this is consistent with the cysteine to serine mutation in *Chromatium vinosum* HiPIP, where the better electron donor serine stabilizes an Fe^{3+} over an $Fe2.5^+$.[53–56]

Moreover, along the fission pathway of the clusters, the difference in the spin densities between the two irons on a layer of all homo- and hetero-ligand clusters significantly increased, consequently resulting in two Fe^{3+}-Fe^{2+} pairs for the half-cleaved intermediates (Figure 4, Table S3 and Table S4). Since the degree of localization for the $[Fe_4S_4(SMe,L)_2]^{2-}$ reactant was greater and thus closer to that for its spin-localized transition state (Table S3), the activation barrier of the cleavage for these clusters should be lower with respect to other clusters.

Energetics of Cleavage

The energetics of the cleavage mechanism in the hetero-ligand relative to homo-ligand clusters was examined for the steps of the cluster fission to the half-cleaved structure. Our previous DFT studies[28] revealed a low-barrier mechanism (Scheme 3), in which the spin-delocalized [4Fe-4S] parent goes through a spin-localized transition structure, followed by a half-cleaved cluster through cleavage perpendicular to the layers of the two weak Fe^{2+}—S bonds, and finally proceeds to the [2Fe-2S] fission product. However, although spin-localized intermediates for $[Fe_4S_4Cl_4]^{2-}$ and $[Fe_4S_4H_4]^{2-}$, in which the minority spins were excited to the spin polarized $\delta_{Fe—Fe}$ orbitals, were isolated by the BS-DFT calculations, optimization of this intermediate for $[Fe_4S_4(SCH_3)_4]^{2-}$ fails to converge and slides smoothly to the spin-delocalized state. Further intrinsic reaction coordinate calculations and Hessian analysis of the transition state optimization suggest that the cleavage of the spin-delocalized $[Fe_4S_4L_4]^{2-}$ proceeds through a spin-localized transition state directly, in which the minority spins have polarized $\sigma_{Fe—Fe}$ bonding character, to the half-cleaved structure. Thus, here the energetics of the spin-delocalized reactant, the spin-localized transition state, and the half-cleaved structure (Scheme

3) of $[Fe_4S_4L_4]^{2-}$ and $[Fe_4S_4(SCH_3)_2L_2]^{2-}$ (L = SCH_3, Cl, H) are compared (Table 2, Table S5, and Figure 5). Both energies and free energies are reported; however, since the energies are the relevant quantities for the CID experiments, the focus is on the energies.

For the reaction to the half-cleaved species, the homo-ligand clusters $[Fe_4S_4Cl_4]^{2-}$and $[Fe_4S_4(SCH_3)_4]^{2-}$ had similar activation energy $\Delta E^{\ddagger}$ of ~10 kcal/mol and reaction energy ΔE of ~8.4 kcal/mol while the cleavage reaction of $[Fe_4S_4H_4]^{2-}$ was only endothermic by 3.3 kcal/mol with a lower $\Delta E^{\ddagger}$ of 6.0 kcal/mol (Figure 5). The cleavage of $[Fe_4S_4H_4]^{2-}$ was much easier than the other homodimers apparently because the Fe—S bonds were longer by ~ 0.014 — 0.019 Å relative to the other homodimers.

The cleavage of hetero-ligand clusters was complicated by the two possible isomers, $[Fe_4S_4(SMe)_2L_2]^{2-}$ and $[Fe_4S_4(SMe,L)_2]^{2-}$, the latter being more stable by 0.87 and 0.81 kcal/mol for L = H and Cl, respectively. Moreover, the cleavage of $[Fe_4S_4(SMe,L)_2]^{2-}$ was further complicated by having three distinct cleavage pathways (Scheme 4), each with distinct reactivity and selectivity. Specifically, mechanism **a** involves cleavage through Fe_2—S_2 and Fe_4—S_4, in which the Fe are coordinated by either L = H or Cl, mechanism **c** involves cleavage through Fe_1—S_1 and Fe_3—S_3, in which the Fe are coordinated by SMe, and mechanism **b** involves cleavage through either Fe_1—S_2 and Fe_3—S_4 or Fe_2—S_1 and Fe_4—S_3, in which one Fe is coordinated by L and the other by SMe. The pathways involving cleavage through Fe^{2+}—S bonds are expected to be most favored, with spin density patterns of the transition state and half-cleaved intermediate most similar to the reactant.

The fission of $[Fe_4S_4(SCH_3)_2Cl_2]^{2-}$ was first compared with that of $[Fe_4S_4Cl_4]^{2-}$and $[Fe_4S_4(SCH_3)_4]^{2-}$ (Figure 5 and Table 2). The $[Fe_4S_4(SMe)_2Cl_2]^{2-}$ isomer had one layer that looks like the $[Fe_4S_4Cl_4]^{2-}$ layers and the other like the $[Fe_4S_4(SCH_3)_4]^{2-}$ layers because the ligands are symmetric for a given layer. Since the two homodimers had similar $\Delta E^{\ddagger}$, the $[Fe_4S_4(SMe)_2Cl_2]^{2-}$ isomer also had similar $\Delta E^{\ddagger}$ to them. On the other hand, the minority spin was more localized for $[Fe_4S_4(SMe,Cl)_2]^{2-}$ than the two homodimers since the spin density was less on Fe_2 and Fe_4 coordinated by the Cl^- ligands than the other two ions, increasing their Fe^{2+} character (Figure 3 and 4). $\Delta E^{\ddagger}$ and ΔE were consistent with easier cleavage through Fe^{2+}—S bonds; i.e., 8.6 and 6.7 kcal/mol, respectively, for mechanism **a** with cleavage through two Fe^{2+}—S bonds, slightly larger at 8.6 and 7.5 kcal/mol, respectively, for mechanism **b** with cleavage through one Fe^{2+}— S bond, and with significantly larger values for mechanism **c** and the other isomer with no Fe^{2+}—S bonds. Overall, the expected pathway of cleavage of $[Fe_4S_4(SCH_3)_2Cl_2]^{2-}$ was through mechanism **a** and **b** of $[Fe_4S_4(SMe,Cl)_2]^{2-}$ (Figure 5). Moreover, since the $\Delta E^{\ddagger}$ was about 1.5 kcal/mol lower for these two mechanisms than that of the two homodimers, cleavage of the heterodimer should be easier than of either homodimer. In fact, fission at low collision energies (E_{CM}) is observed in CID experiments for $[Fe_4S_4(SCH_3)_2Cl_2]^{2-}$ (at E_{CM} = 0.81 eV) but not for $[Fe_4S_4(SCH_3)_4]^{2-}$ (at E_{CM} = 0.75 eV) or for $[Fe_4S_4Cl_4]^{2-}$.[31,36] Fission of $[Fe_4S_4Cl_4]^{2-}$ is observed at slightly higher energies (at E_{CM} = 1.75 eV)[31,36] , but fission of $[Fe_4S_4(SCH_3)_4]^{2-}$ is not observed until much higher energies.[31,36]

The fission of $[Fe_4S_4(SCH_3)_2H_2]^{2-}$ was also compared with $[Fe_4S_4(SCH_3)_4]^{2-}$ and $[Fe_4S_4H_4]^{2-}$. Unlike the previous case, the two homodimers differ from each other by more than 4 kcal/mol in $\Delta E^{\ddagger}$ and ΔE (Figure 5 and Table 2). However, like the $[Fe_4S_4(SMe,Cl)_2]^{2-}$ isomer, the $[Fe_4S_4(SMe)_2H_2]^{2-}$ isomer had similar spin-delocalization pattern for each layer and so the energetics are intermediate between the two homodimers because one set of bonds was like one homodimer and the other set like the other homodimer. For $[Fe_4S_4(SMe,H)_2]^{2-}$, the spin density was significantly less on Fe1 and Fe_3 coordinated by the H^- ligands than the other two irons, increasing their Fe^{2+} character (Figure 3 and 4). Here again the $\Delta E^{\ddagger}$ and ΔE were consistent with easier cleavage through Fe^{2+}—S bonds; i.e., 5.6

and 4.5 kcal/mol, respectively, for mechanism **c** with cleavage through two Fe^{2+}—S bonds, 6.9 and 5.3 kcal/mol for mechanism **b** with cleavage through one Fe^{2+}—S bond, and much larger values for mechanism **a** and the other isomer with no Fe^{2+}—S bonds. Moreover, these energies were smaller than those for chloride ligands, indicating that the greater difference in the spin density of the iron sites ligated by hydrides over those ligated by the chlorides promoted the cleavage. However, it is important to note that the effects of spin localization for either the hydride or chloride led to the greatest promotion of cleavage regardless of the nature of the ligand. Although there are no experimental results, the expected fission pathway is through mechanism **c** and **b** of $[Fe_4S_4(SMe,Cl)_2]^{2-}$ (Figure 5 and Table 2).

Conclusions

To elucidate whether the fission of [4Fe-4S] cluster to two [2Fe-2S] clusters proceeds through a half-cleaved intermediate favored by minority spin-localization, the cubic homo-ligand $[Fe_4S_4L_4]^{2-}$ (L = SCH_3, Cl, H) and hetero-ligand $[Fe_4S_4(SCH_3)_2L_2]^{2-}$ (L = Cl, H) clusters were investigated using BS-DFT calculations in conjunction with results of X-ray, PES, and CID experiments. First, the results indicate that the substitution of chloride or hydride ligands for one of the two irons of a layer of $[Fe_4S_4(SCH_3)_4]^{2-}$ causes spin localization. Thus, while the irons in a layer with two homo-ligands still remain a symmetric $Fe^{2.5+}$—$Fe^{2.5+}$ pair, the irons in a layer with two hetero-ligands form an Fe^{3+}—Fe^{2+} pair. Second, the Fe^{2+}/Fe^{3+} character of an iron, as determined by the Fe—S bond lengths, charge density, and the degree of spin localization, correlates with electron donating ability of the ligands. In a layer with homo-ligands, the Fe^{2+} character of an iron slightly increases with increasing electron donating ability of its ligand because electron density simply shifts from the ligand to the iron. On the other hand, in a layer with hetero-ligands, the Fe^{2+} character of an iron significantly increases with *decreasing* electron donating ability of its ligand because even though less electron density shifts to the iron ligated by a poorer electron donor ligand, the minority spin is attracted to it, resulting in overall greater Fe^{2+} character. Third, the reactivity of clusters in the cleavage reaction apparently correlates with the Fe^{2+} character of the Fe—S bonds. Therefore, the $[Fe_4S_4(SMe,L)_2)]^{2-}$ isomers have a lower $\Delta E^{\ddagger}$ compared to the corresponding homodimers for the lowest energy pathway in which the two Fe—S bonds being broken have Fe^{2+} character. The results for the clusters with the chloride ligands are especially compelling since both homo-ligand clusters $[Fe_4S_4Cl_4]^{2-}$ and $[Fe_4S_4(SCH_3)_4]^{2-}$ have approximately the same $\Delta E^{\ddagger}$ but the hetero-ligand cluster $[Fe_4S_4(SCH_3)_2Cl_2]^{2-}$ is predicted to be much easier to cleave, which is consistent with the CID experimental results.[31] Cleavage mainly via the pathway resulting in $[Fe_2S_2(SCH_3)Cl]^{-}$ (pathway **a**) and somewhat less via the pathway resulting in $[Fe_2S_2Cl_2]^{2-}$ and $[Fe_2S_2(SCH_3)_2]^{-}$ (pathway **b**) is also consistent with the CID results.[31,36]

Overall, our calculations along with the CID results support the hypothesis that the symmetric fission of [4Fe-4S] clusters occurs via a spin localized transition structure. Furthermore, proteins requiring facile fission of their clusters for their biological function such as the scaffold proteins for Fe-S cluster assembly might have protein environments that promote spin localization. Therefore, further experimental and theoretical investigations of the effects of ligand substitution and spin localization on the cleavage of [4Fe-4S] clusters are important in elucidating the function of many [4Fe-4S] proteins.

Supplementary Material

Refer to Web version on PubMed Central for supplementary material.

Acknowledgment

We thank Prof. Lai-Sheng Wang, Dr. You-Jun Fu, and Dr. Xuebin Wang for the detailed experimental data and valuable discussions. This work was supported by the National Institutes of Health (GM-45303). The calculations were performed at the Environmental Molecular Sciences Laboratory, a national user facility sponsored by the U.S. DOE's Office of Biological and Environmental Research and located at Pacific Northwest National Laboratory, operated for DOE by Battelle, under the grant GC3565 and GC20901. Additional computational resources were provided by the William G. McGowan Foundation.

References

1. Beinert H, Holm RH, Munck E. Science 1997;277:653. [PubMed: 9235882]
2. Spiro, TG., editor. Iron—Sulfur Proteins. Vol. Vol. IV.. New York: 1982.
3. Beinert HJ. Biol. Inorg. Chem 2000;5:2.
4. Adman E, Watenpaugh KD, Jensen LH. Proc. Natl. Acad. Sci. U. S. A 1975;72:4854. [PubMed: 1061073]
5. Kassner RJ, Yang WJ. Am. Chem. Soc 1977;99:4351.
6. Stephens PJ, Jollie DR, Warshel A. Chem. Rev 1996;96:2491. [PubMed: 11848834]
7. Sheridan RP, Allen LC, Carter CWJJ. Biol. Chem 1981;256:5052.
8. Backes G, Mino Y, Loehr TM, Meyer TE, Cusanovich MA, Sweeny WV, Adman ET, Sanders-Loehr JJ. Am. Chem. Soc 1991;113:2055.
9. Banci L, Bertini I, Gori Savellini G, Luchinat C. Inorg. Chem 1996;35:4248. [PubMed: 11666635]
10. Babini E, Borsari M, Capozzi F, Eltis LD, Luchinat CJ. Biol. Inorg. Chem 1999;4:692.
11. Beck BW, Xie Q, Ichiye T. Biophys. J 2001;81:601. [PubMed: 11463610]
12. Glaser T, Bertini I, Moura JJ, Hedman B, Hodgson KO, Solomon EIJ. Am. Chem. Soc 2001;123:4859.
13. Beinert H, Kiley PJ. Curr. Opin. Chem. Biol 1999;3:152. [PubMed: 10226040]
14. Beinert H, Kennedy MC, Stout CD. Chem. Rev 1996;96:2335. [PubMed: 11848830]
15. Flint DH, Allen RM. Chem. Rev 1996;96:2315. [PubMed: 11848829]
16. Krebs C, Agar JN, Smith AD, Frazzon J, Dean DR, Huynh BH, Johnson MK. Biochem 2001;40:14069. [PubMed: 11705400]
17. Smith AD, Jameson GN, Dos Santos, PC., Agar JN, Naik S, Krebs C, Frazzon J, Dean DR, Huynh BH, Johnson MK. Biochem 2005;44:12955. [PubMed: 16185064]
18. Agar JN, Krebs C, Frazzon J, Huynh BH, Dean DR, Johnson MK. Biochem 2000;39:7856. [PubMed: 10891064]
19. Ding H, Clark RJ. Biochem. J 2004;379:433. [PubMed: 14720122]
20. Ding H, Clark RJ, Ding BJ. Biol. Chem 2004;279:37499.
21. Wollenberg M, Berndt C, Bill E, Schwenn JD, Seidler A. Eur. J. Biochem 2003;270:1662. [PubMed: 12694179]
22. Berndt C, Lillig CH, Wollenberg M, Bill E, Mansilla MC, de Mendoza, D., Seidler A, Schwenn JDJ. Biol. Chem 2004;279:7850.
23. Dos, Santos; P. C., Smith, AD.; Frazzon, J.; Cash, VL.; Johnson, MK.; Dean, DRJ. Biol. Chem 2004;279:19705.
24. Sen S, Igarashi R, Smith A, Johnson MK, Seefeldt LC, Peters JW. Biochem 2004;43:1787. [PubMed: 14967020]
25. Noodleman L, Peng CY, Case DA, Mouesca JM. Coord. Chem. Rev 1995;144:199.
26. Wang X-B, Niu S-Q, Yang X, Ibrahim SK, Pickett CJ, Ichiye T, Wang L-SJ. Am. Chem. Soc 2003;125:14072.
27. Yang X, Wang X-B, Niu S, Pickett CJ, Ichiye T, Wang L-S. Phys. Rev. Lett 2002;89:163401. [PubMed: 12398720]
28. Niu S-Q, Wang X-B, Yang X, Wang L-S, Ichiye TJ. Phys. Chem. A 2004;108:6750.
29. Niu S-Q, Ichiye TTheor. Chim. Acta 2007;117:275.
30. Yang X, Wang XB, Wang LSIntJMass. Spectrom 2003;228:797.

31. Fu YJ, Laskin J, Wang LSIntJMass. Spectrom 2006;255:102.
32. Fu YJ, Laskin J, Wang LSIntJMass. Spectrom 2007;263:260.
33. Zhai HJ, Yang X, Fu YJ, Wang XB, Wang LSJ. Am. Chem. Soc 2004;126:8413.
34. Fu YJ, Yang X, Wang XB, Wang LS. Inorg. Chem 2004;43:3647. [PubMed: 15180419]
35. Fu Y-J, Niu S-Q, Ichiye T, Wang L-S. Inorg. Chem 2005;44:1202. [PubMed: 15732958]
36. Fu YJ, Yang X, Wang XB, Wang LSJ. Phys. Chem. A 2005;109:1815.
37. Niu S-Q, Wang X-B, Nichols JA, Wang L-S, Ichiye TJ. Phys. Chem. A 2003;107:2898.
38. Niu S-Q, Nichols JA, Ichiye T. Unpublished work. 2008
39. Yang X, Niu SQ, Ichiye T, Wang LSJ. Am. Chem. Soc 2004;126:15790.
40. Fu YJ, Niu SQ, Yang X, Wang XB, Ichiye T, Wang LS. unpublished
41. George SJ, Armstrong FA, Hatchikian EC, Thomson AJ. Biochem. J 1989;264:275. [PubMed: 2557832]
42. Thomson AJ, Breton J, Butt JN, Hatchikian EC, Armstrong FAJ. Inorg. Biochem 1992;47:197.
43. Conover RC, Kowal AT, Fu WG, Park JB, Aono S, Adams MW, Johnson MKJ. Biol. Chem 1990;265:8533.
44. Gorst CM, Yeh YH, Teng Q, Calzolai L, Zhou ZH, Adams MW, La Mar GN. Biochem 1995;34:600. [PubMed: 7819255]
45. Calzolai L, Gorst CM, Zhao ZH, Teng Q, Adams MW, La Mar GN. Biochem 1995;34:11373. [PubMed: 7547865]
46. Busch JL, Breton JL, Bartlett BM, Armstrong FA, James R, Thomson AJ. Biochem. J 1997;323:95. [PubMed: 9173907]
47. Walsby CJ, Ortillo D, Yang J, Nnyepi MR, Broderick WE, Hoffman BM, Broderick JB. Inorg. Chem 2005;44:727. [PubMed: 15859242]
48. Cheek J, Broderick JBJ. Biol. Inorg. Chem 2001;6:209.
49. Fontecave M, Mulliez E, Ollagnier-de-Choudens S. Curr. Opin. Chem. Biol 2001;5:506. [PubMed: 11578923]
50. Jarrett JT. Curr. Opin. Chem. Biol 2003;7:174. [PubMed: 12714049]
51. Frey PA, Magnusson OT. Chem. Rev 2003;103:2129. [PubMed: 12797826]
52. Jarrett JT. Arch. Biochem. Biophys 2005;433:312. [PubMed: 15581586]
53. Dilg AWE, Capozzi F, Mentler M, Iakovleva O, Luchinat C, Bertini I, Parak FGJ. Biol. Inorg. Chem 2001;6:232.
54. Dilg AWE, Grantner K, Iakovleva O, Parak FG, Babini E, Bertini I, Capozzi F, Luchinat C, Meyer-Klaucke WJ. Biol. Inorg. Chem 2002;7:691.
55. Dilg AWE, Mincione G, Achterhold K, Iakovleva O, Mentler M, Luchinat C, Bertini I, Parak FGJBiol. Inorg. Chem 1999;4:727.
56. Babini E, Bertini I, Borsari M, Capozzi F, Dikiy A, Eltis LD, Luchinat CJ. Am. Chem. Soc 1996;118:75.
57. Noodleman LJ. of Chem. Phys 1981;74:5737.
58. Noodleman L, Case DA. Adv. Inorg. Chem 1992;38:423.
59. Parr, RG.; Yang, W. Density-functional theory of atoms and molecules. Oxford, U.K.: Oxford University Press; 1989.
60. Becke ADJ. Chem. Phys 1993;98:5648.
61. Lee CT, Yang WT, Parr RG. Phys. Rev. B 1988;37:785.
62. Rassolov VA, Pople JA, Ratner MA, Windus TLJ. Chem. Phys 1998;109:1223.
63. Francl MM, Petro WJ, Hehre WJ, Binkley JS, Gordon MS, DeFrees DJ, Pople JAJ. Chem. Phys 1982;77:3654.
64. Hariharan PC, Pople JA. Theor. Chim. Acta 1973;28:213.
65. Schlegel HBJ. Comput. Chem 1982;3:214.
66. Foresman, JB.; Frisch, A. Gaussian Inc. Exploring chemistry with electronic structure methods. Vol. 2nd ed.. Pittsburgh, Pa: Gaussian Inc; 1996.
67. Mouesca JM, Chen JL, Noodleman L, Bashford D, Case DAJ. Am. Chem. Soc 1994;116:11898.

68. Li J. Acta Chimica Sinica 2000;58:1529.

69. Straatsma, TP.; Windus, TL.; Bylaska, EJ.; de Jong, W.; Hirata, S.; Valiev, M.; Hackler, M.; Pollack, L.; Harrison, R.; Dupuis, M.; Smith, DMA.; Nieplocha, JVT.; Krishnan, M.; Auer, AA.; Brown, E.; Cisneros, G.; Fann, G.; Früchtl, H.; Garza, J.; Hirao, K.; Kendall, R.; Nichols, J.; Tsemekhman, K.; Wolinski, K.; Anchell, J.; Bernholdt, D.; Borowski, P.; Clark, T.; Clerc, D.; Dachsel, H.; Deegan, M.; Dyall, K.; Elwood, D.; Glendening, E.; Gutowski, M.; Hess, A.; Jaffe, J.; Johnson, B.; Ju, J.; Kobayashi, R.; Kutteh, R.; Lin, Z.; Littlefield, R.; Long, X.; Meng, B.; Nakajima, T.; Niu, S.; Rosing, M.; Sandrone, G.; Stave, M.; Taylor, H.; Thomas, G.; van Lenthe, J.; Wong, A.; Zhang, Z. A Computational Chemistry Package for Parallel Computers, Version 4.6. Richland, Washington, USA: Pacific Northwest National Laboratory; 2004. 99352–0999

70. Black, G.; Didier, B.; Elsethagen, T.; Feller, D.; Gracio, D.; Hackler, M.; Havre, S.; Jones, D.; Jurrus, E.; Keller, T.; Lansing, C.; Matsumoto, S.; Palmer, B.; Peterson, M.; Schuchardt, K.; Stephan, E.; Taylor, HTG.; Vorpagel, E.; Windus, T.; Winters, C. Ecce, A Problem Solving Environment for Computational Chemistry, Software Version 3.2.1. Richland, Washington, USA: Pacific Northwest National Laboratory; 2004. 99352–0999

71. Lane RW, Ibers JA, Frankel RB, Papaefthymiou GC, Holm RH. J. Am. Chem. Soc 1977;99:84. [PubMed: 830690]

72. Carney MJ, Papaefthymiou GC, Spartalian K, Frankel RB, Holm RH. J. Am. Chem. Soc 1988;110:6084.

73. Osullivan T, Millar MMJ. Am. Chem. Soc 1985;107:4096.

74. Excoffon P, Laugier J, Lamotte B. Inorg. Chem 1991;30:3075.

75. Venkateswara, Rao; P., Holm, RH. Chem. Rev 2004;104:527. [PubMed: 14871134]

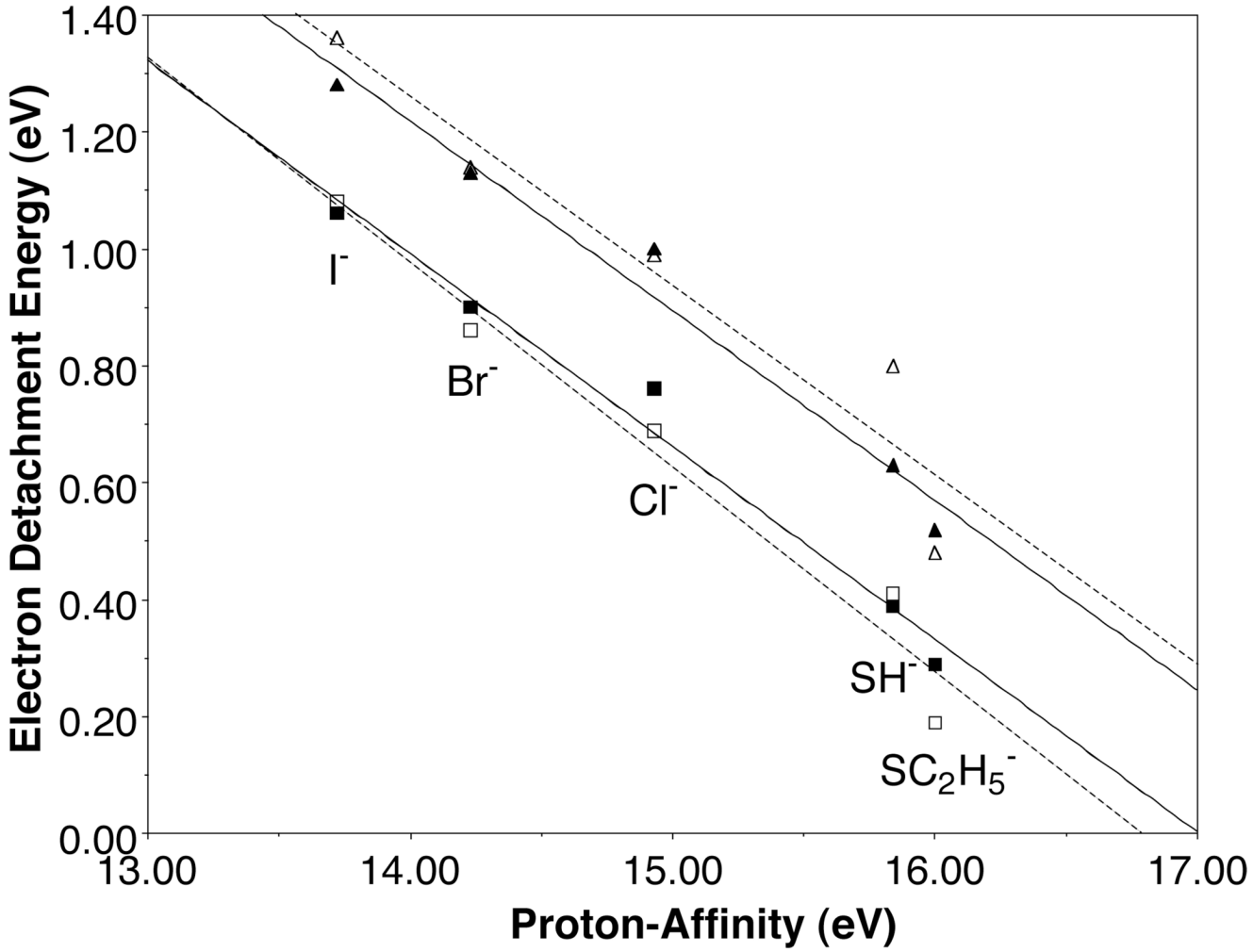

Figure 1.

Calculated (dashed line) ADE (open square) and VDE (open triangle)* and experimental (solid line) ADE (filled square) and VDE (filled triangle) versus proton affinity (PA) for of $[Fe_4S_4L_4]^{2-}$ with L as indicated in the figure. * In the calculations, SC_2H_5 was replaced by a thiolate SCH_3 group.

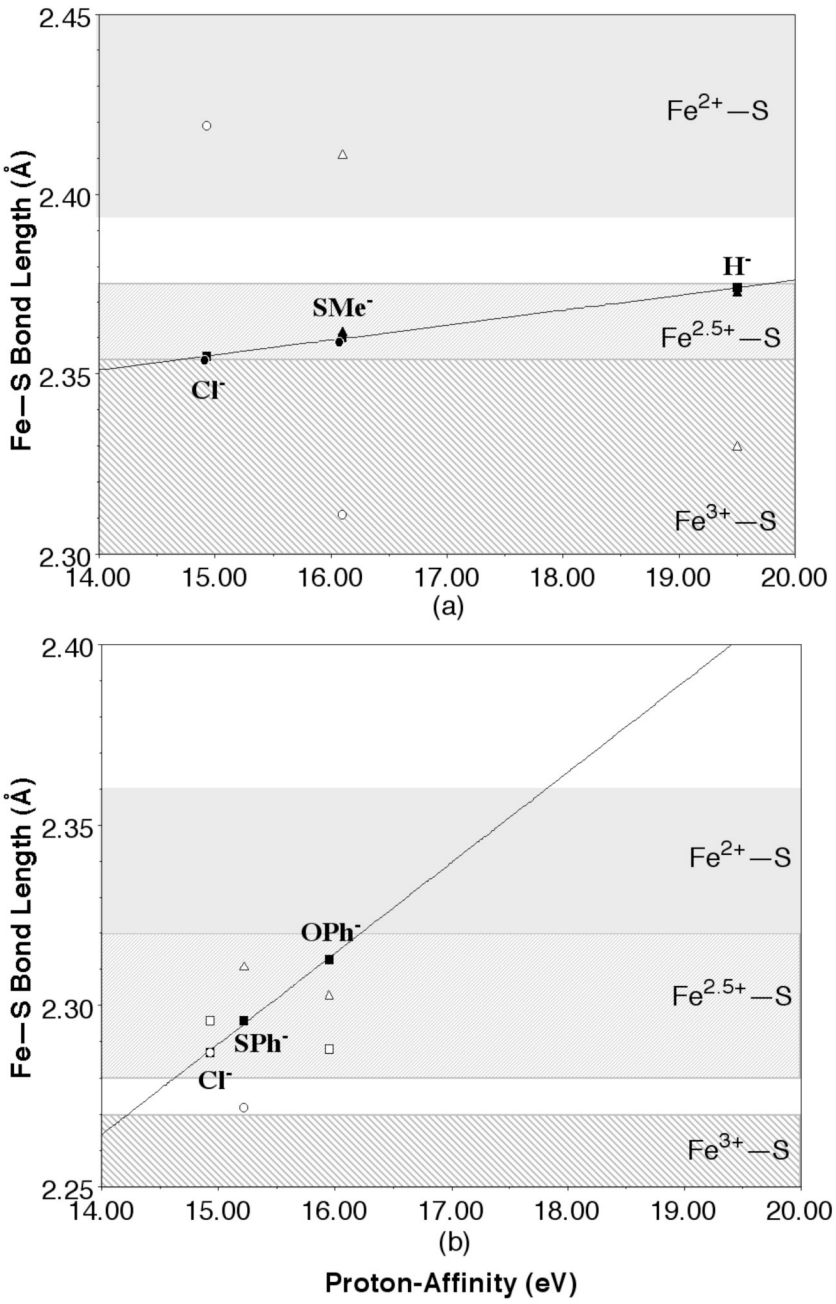

Figure 2.

Scatter plot of cluster Fe—S bond lengths within the layer versus proton affinity (PA) (a) calculated at the B3LYP/6-31G** level for $[Fe_4S_4L_4]^{2-}$ (L = Cl, SMe_3, H; SMe = SCH_3) (filled square); $[Fe_4S_4(SMe)_2L_2]^{2-}$, L = Cl (filled circle), H (filled triangle); and $[Fe_4S_4(SMe,L)_2]^{2-}$, L = Cl (open circle), H (open triangle) and (b) measured by X-ray for $[Fe_4S_4L_4]^{2-}$, L = Cl, SPh, OPh (filled square), Ph = phenyl; $[Fe_4S_4(SPh,L)_2]^{2-}$, L = Cl (open circle), OPh (open triangle); and $[Fe_4S_4(OPh,Cl)_2]^{2-}$ (open square). The correlation line is for the $[Fe_4S_4L_4]^{2-}$ only.

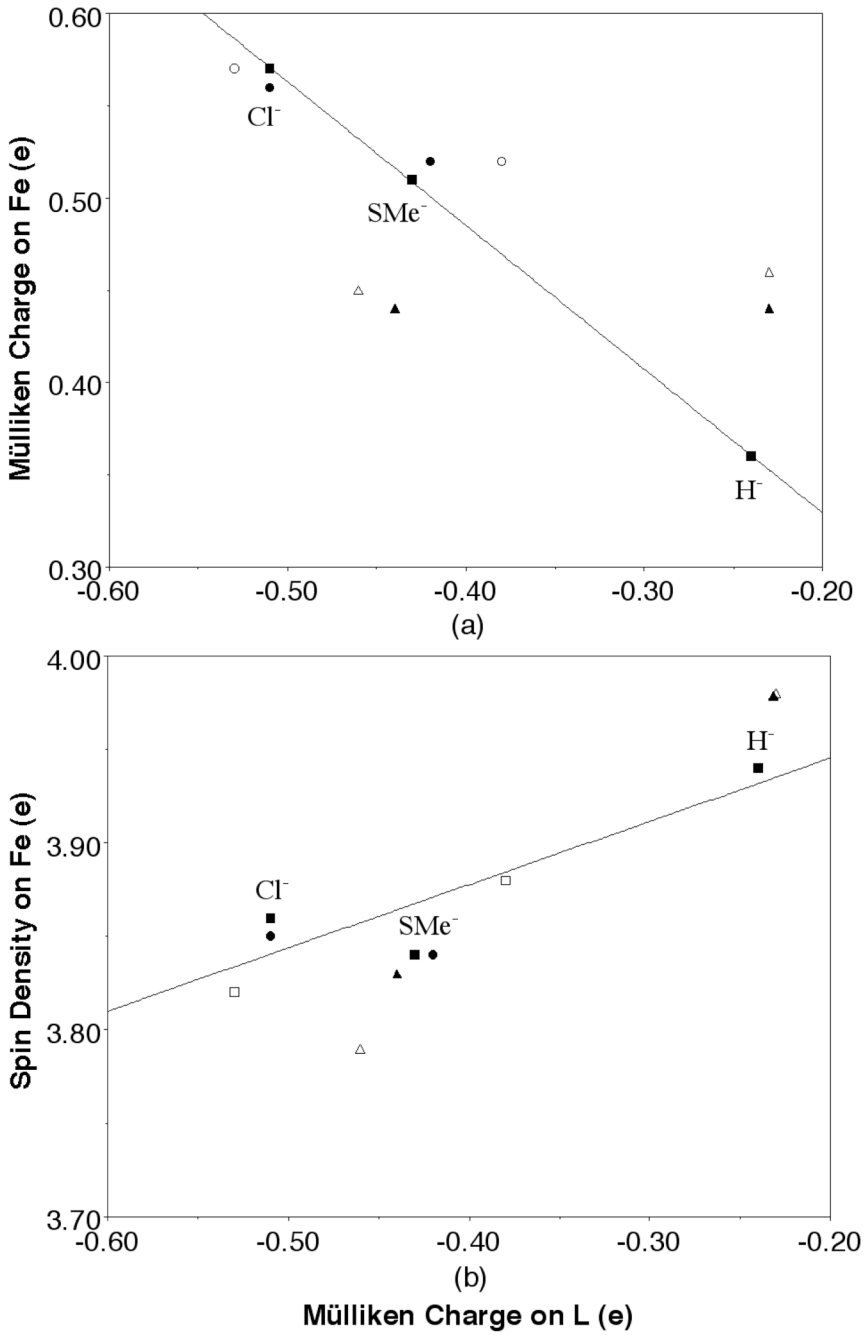

Figure 3.

Scatter plot of the calculated Mülliken charge on ligand versus (a) Mülliken charge on irons and (b) Mülliken spin density on irons at the B3LYP/6-31G** level for $[Fe_4S_4L_4]^{2-}$ (L = Cl, SMe_3, H; SMe = SCH_3) (filled square); $[Fe_4S_4(SMe)_2L_2]^{2-}$, L = Cl (filled circle), H (filled triangle); and $[Fe_4S_4(SMe,L)_2]^{2-}$, L = Cl (open circle), H (open triangle). The correlation line is for the $[Fe_4S_4L_4]^{2-}$ only.

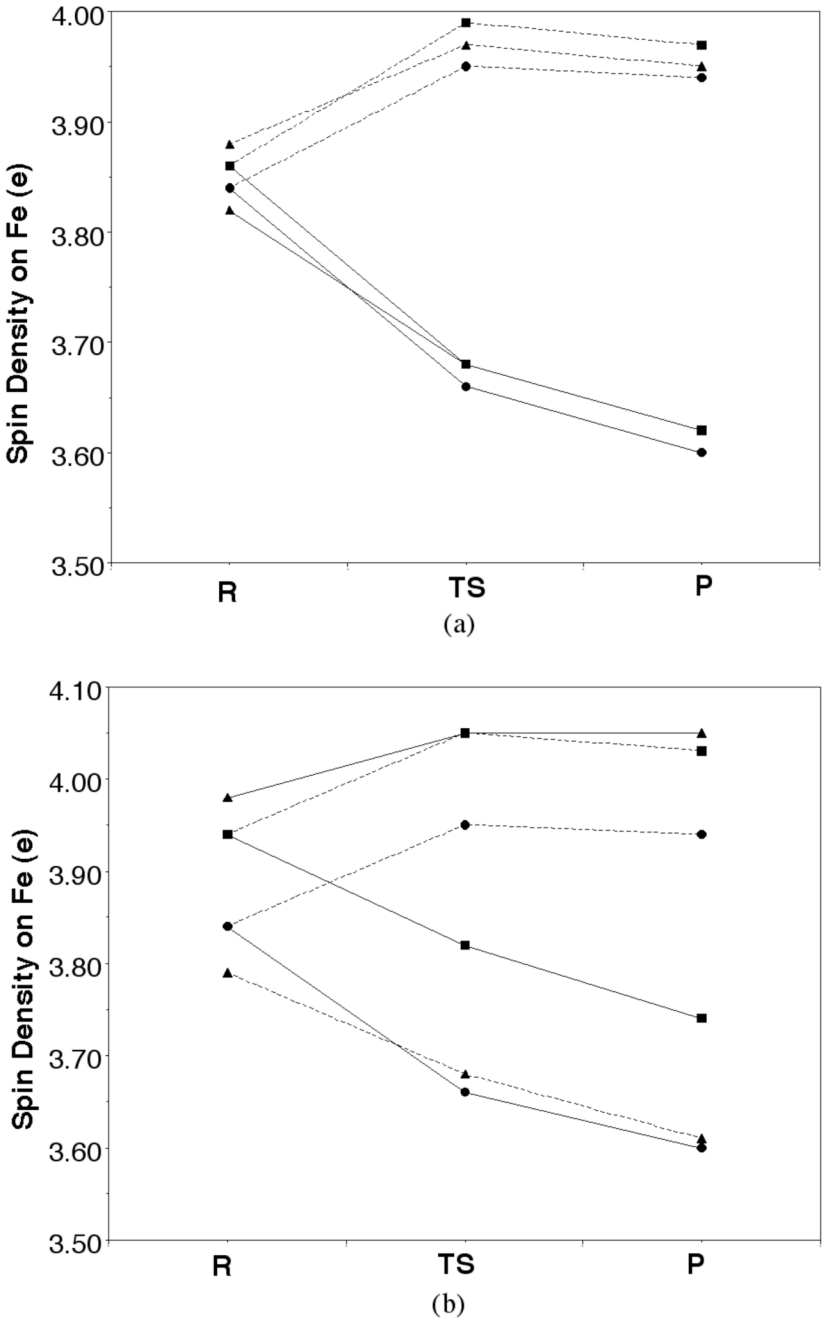

Figure 4.

Change of spin density on Fe_3 (solid line) and Fe_4 (dashed line) of $[Fe_4S_4L_4]^{2-}$, L = SMe (filled circle) and Cl (filled square), $[Fe_4S_4(SMe,Cl)_2]^{2-}$ (filled triangle) (a); and $[Fe_4S_4L_4]^{2-}$, L = Me (filled circle) and H (filled square), $[Fe_4S_4(SMe,H)_2]^{2-}$ (filled triangle) (b) along cleavage reaction pathway from the cubic reactant (**R**) through transition state (**TS**) to the half-cleaved product(**P**).

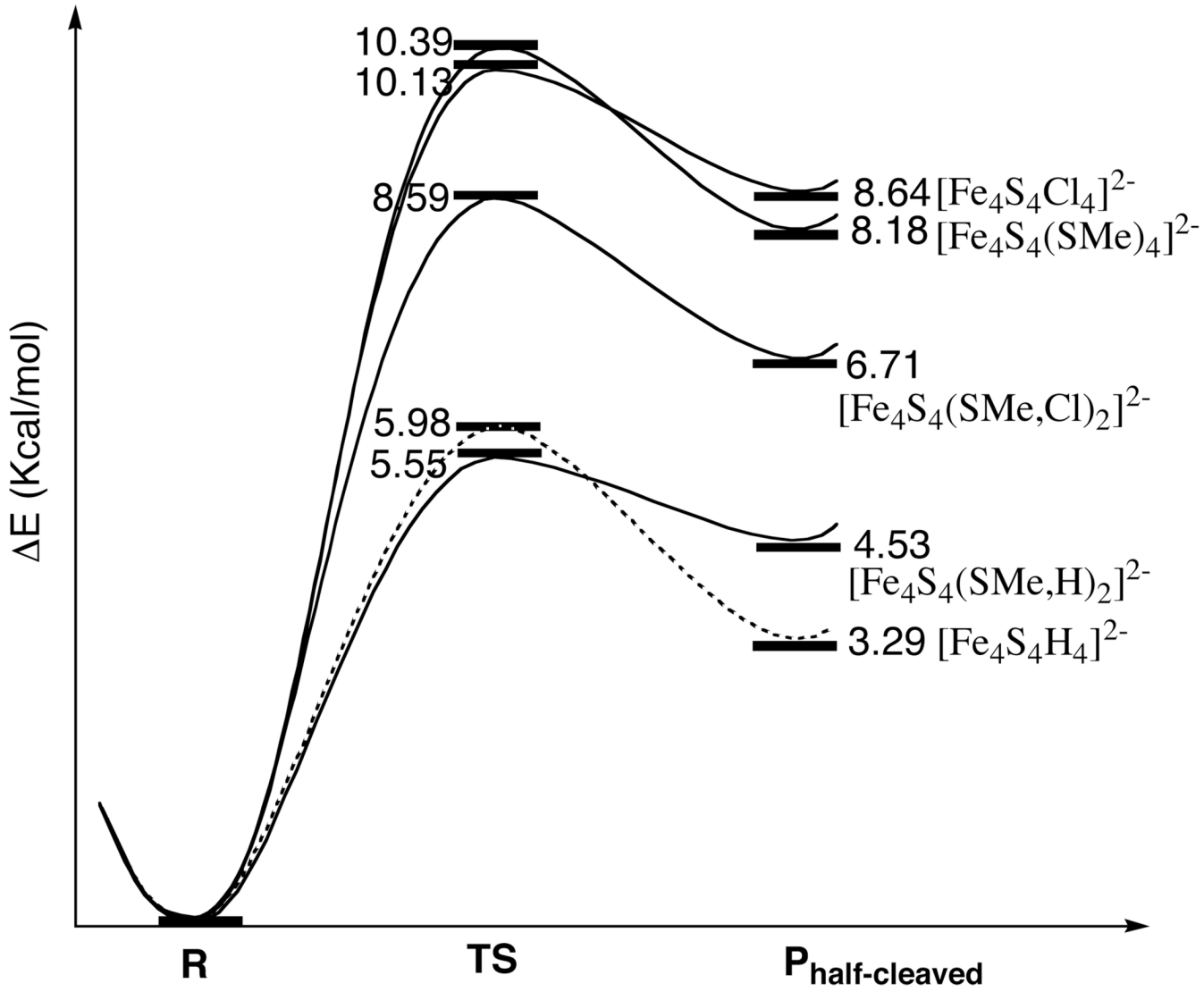

Figure 5.
The calculated cleavage activation and reaction energies of $[Fe_4S_4L_4]^{2-}$ and $[Fe_4S_4(SMe,L)_2]^{2-}$ (L = SMe, H, Cl) along the lowest energy pathway from the cubic reactant (**R**) through transition state (**TS**) to the half-cleaved product (**P**).

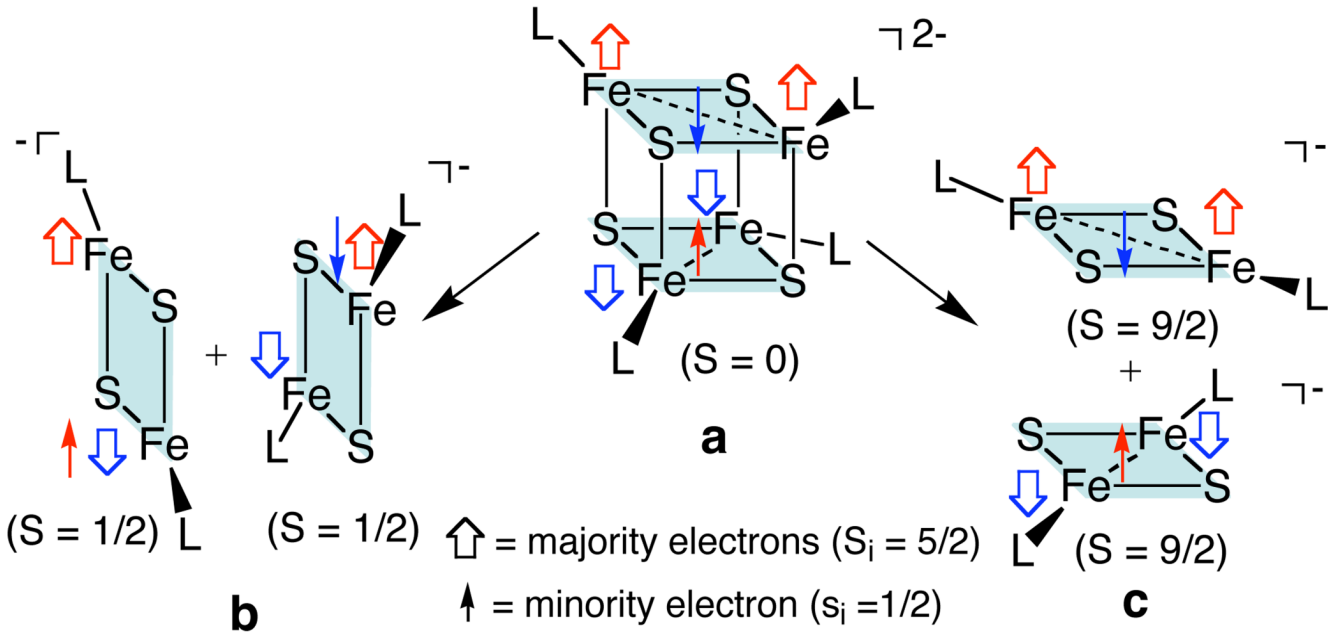

Scheme 1.

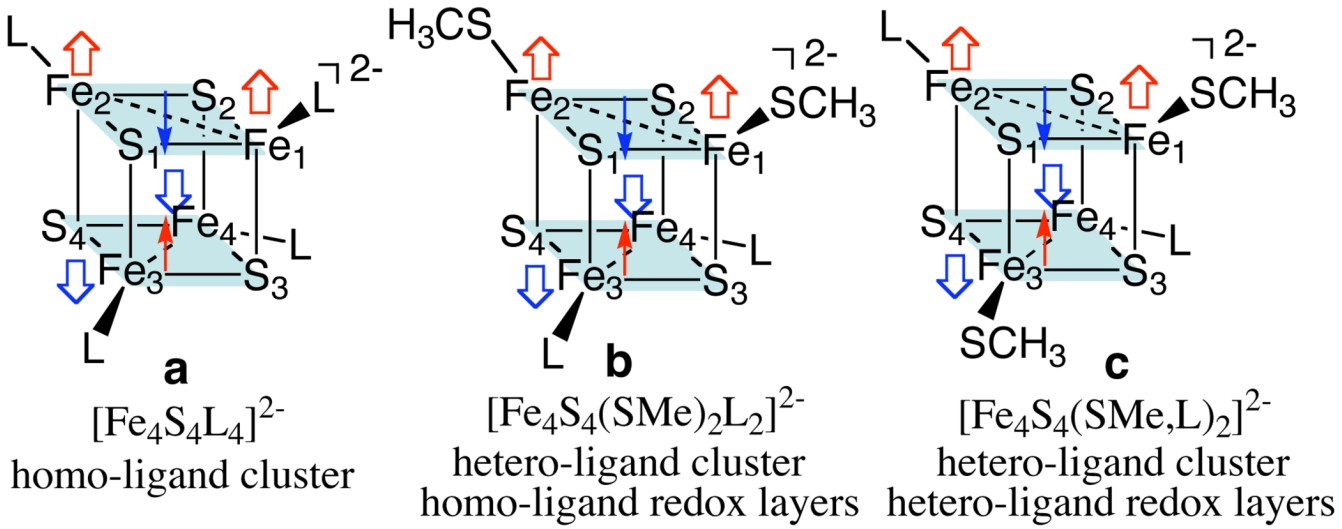

Scheme 2.

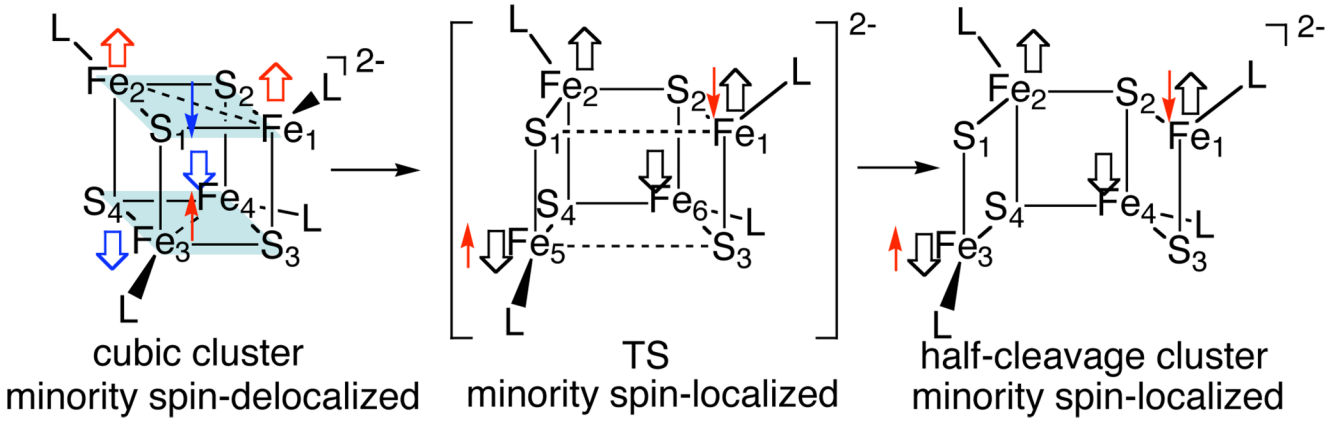

Scheme 3.

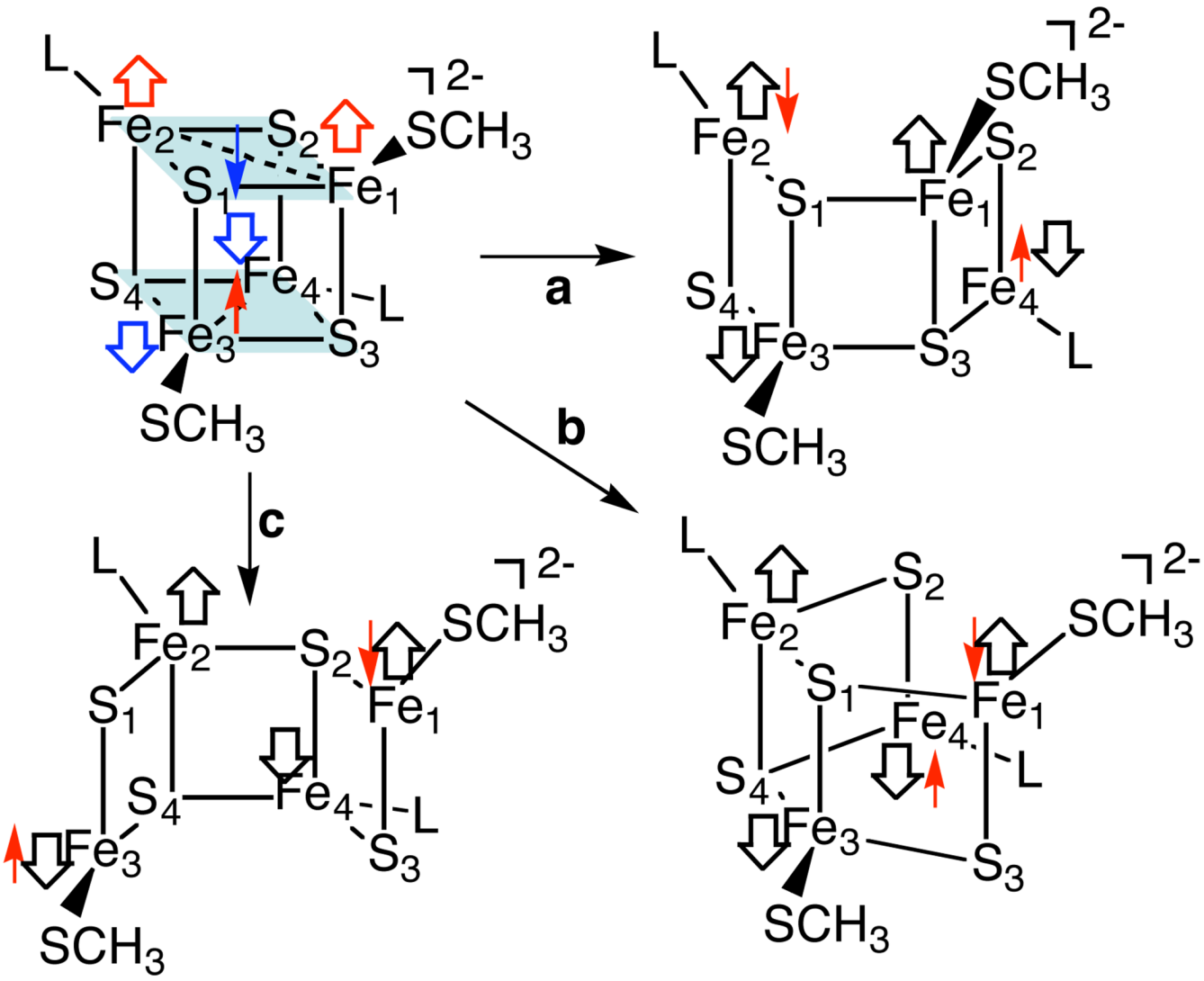

Scheme 4.

Table 1

The B3LYP/6–31(++)$_S$G** and Experimental Adiabatic (ADE) and Vertical (VDE) Detachment Energies (in eV) of the Intact $[Fe_4S_4L_4]^{2-}$ and $[Fe_4S_4(SCH_3)_2L_2]^{2-}$ (L = SCH_3, Cl, H; SMe = SCH_3) Clusters.

	ADE			VDE		
	L_1L_2[a]	L_3L_4[b]	exp[c]	L_1L_2	L_3L_4	exp[c]
			0.29(8)[d]			0.52(6)
$[Fe_4S_4(SCH_3)_4]^{2-}$	0.16	0.16		0.46	0.46	*d*
$[Fe_4S_4Cl_4]^{2-}$	0.69	0.69	0.80(8)	0.99	0.99	1.01(6)
$[Fe_4S_4H_4]^{2-}$	−0.49	−0.49		−0.12	−0.12	
$[Fe_4S_4(SMe)_2Cl_2]^{2-}$	0.45	0.32		0.78	0.70	
			0.52(8)[d]			0.71(6)
$[Fe_4S_4(SMe,Cl)_2]^{2-}$	0.39	0.39		0.74	0.74	*d*
$[Fe_4S_4(SMe)_2H_2]^{2-}$	−0.16	−0.12		0.12	0.22	
$[Fe_4S_4(SMe,H)_2]^{2-}$	−0.11	−0.11		0.21	0.21	

[a] The electron detachment involves the layer ligated by L_1 and L_2

[b] The detachment involves the layer ligated by L_3 and L_4

[c] ref. 26 and 34.

[d] The experimental values are for $[Fe_4S_4(SC_2H_5)_4]^{2-}$ and the DFT calculations indicate that the detachment energies of $[Fe_4S_4(SC_2H_5)_4]^{2-}$ are about 0.03 eV higher than those of $[Fe_4S_4(SCH_3)_4]^{2-}$.

Table 2

The Activation Energies ($\Delta E^{\ddagger}$) and Reaction Energies (ΔE) (in kcal/mol) of the Cleavage of the $[Fe_4S_4L_4]^{2-}$ and $[Fe_4S_4(SCH_3)_2L_2]^{2-}$ (L = SCH_3, Cl, H; SMe = SCH_3) Clusters to the Half-Cleaved Intermediate at the B3LYP/6-31G** Level.

	$\Delta E^{\ddagger}$	$\Delta G^{\ddagger}$	ΔE	ΔG
$[Fe_4S_4(SCH_3)_4]^{2-}$	10.39	8.68	8.18	4.04
$[Fe_4S_4Cl_4]^{2-}$	10.13	9.37	8.64	7.74
$[Fe_4S_4H_4]^{2-}$	5.98	4.85	3.29	1.45
$[Fe_4S_4(SMe)_2Cl_2]^{2-}$	10.46	11.44	7.94	8.00
$[Fe_4S_4(SMe,Cl)_2]^{2-}$ **a**	8.59	8.56	6.71	4.19
$[Fe_4S_4(SMe,Cl)_2]^{2-}$ **b**	8.62	7.95	7.49	6.39
$[Fe_4S_4(SMe,Cl)_2]^{2-}$ **c**	11.14	10.71	10.54	9.91
$[Fe_4S_4(SMe)_2H_2]^{2-}$	7.42	9.03	5.13	5.17
$[Fe_4S_4(SMe,H)2]^{2-}$**a**	10.06	8.77	7.75	4.29
$[Fe_4S_4(SMe,H)_2]^{2-}$**b**	6.90	6.16	5.28	3.64
$[Fe_4S_4(SMe,H)_2]^{2-}$**c**	5.55	5.31	4.53	2.82